Time-dependent density functional theory Ehrenfest dynamics: Collisions between atomic oxygen and graphite clusters

Christine M. Isborn, Xiaosong Li, and John C. Tully

Citation: J. Chem. Phys. **126**, 134307 (2007); doi: 10.1063/1.2713391
View online: http://dx.doi.org/10.1063/1.2713391
View Table of Contents: http://jcp.aip.org/resource/1/JCPSA6/v126/i13
Published by the American Institute of Physics.

Time-dependent density functional theory Ehrenfest dynamics: Collisions between atomic oxygen and graphite clusters

Christine M. Isborn and Xiaosong Li[a)]
Department of Chemistry, University of Washington, Seattle, Washington 98195-1700

John C. Tully
Department of Chemistry, Yale University, New Haven, Connecticut 06520

(Received 14 November 2006; accepted 9 February 2007; published online 3 April 2007)

An *ab initio* direct Ehrenfest dynamics method with time-dependent density functional theory is introduced and applied to collisions of 5 eV oxygen atoms and ions with graphite clusters. Collisions at three different sites are simulated. Kinetic energy transfer from the atomic oxygen to graphite local vibrations is observed and electron-nuclear coupling resulting in electronic excitation within the graphite surface as well as alteration of the atomic charge is first reported in this paper. The three oxygen species studied, $O(^3P)$, $O^-(^2P)$, and $O^+(^4S)$, deposit different amounts of energy to the surface, with the highest degree of damage to the π conjugation of the cluster produced by the atomic oxygen cation. Memory of the initial charge state is not lost as the atom approaches, in contrast to the usual assumption. © *2007 American Institute of Physics*. [DOI: 10.1063/1.2713391]

I. INTRODUCTION

The study of collisions between atoms/molecules and surfaces has been an area of enthusiastic research since surfaces became a topic of interest for the catalysis industry. The interest has continued with the application of surfaces to new developments in electronics and semiconductor technologies, to studying atmospheric processes, and to the erosion of surfaces. A theoretical understanding of the mechanism of charge and energy transfer in ion-surface collision processes will provide insight relevant to many aspects of surface science.

Surface processes often involve multiple potential energy surfaces, and therefore cannot be described by the Born-Oppenheimer or extended Lagrangian trajectories,[1–9] where a single electronic potential surface governs the dynamics. However, solving the full time-dependent Schrödinger equation for both electrons and nuclei in a molecule-surface system is computationally prohibitive. Ehrenfest dynamics offers an affordable solution by coupling quantum equations of motion for electrons with classical equations of motion for nuclei via an average potential surface.[10–12] Our recent development of *ab initio* Ehrenfest dynamics with Hartree-Fock theory shows that electronic excitation as a result of electron-nuclear nonadiabatic coupling can be modeled by such a mean field method.[13] However, Hartree-Fock theory often fails to predict reasonable energetics for highly correlated systems, such as a molecule bound to a surface. It is necessary to extend our electronic dynamics to time-dependent density functional theory (TDDFT). In the current paper, we present the development of *ab initio* Ehrenfest direct dynamics with TDDFT using a three time step integrator and an adaptive step size control method.

The new method is applied to studies of collisions between oxygen atoms/ions and graphite clusters. Such reactions are closely related to the erosion and oxidation processes of a polymer coated surface in the low-earth orbit environment, where atomic oxygen species are abundant. While ions incident on a graphite surface will likely undergo chemical reactions primarily at defect sites, we are interested here in studying energy transfer and charge transfer in nonreactive encounters. We therefore model an idealized graphite surface which we represent by a finite-sized cluster.

II. METHOD

A. *Ab initio* direct Ehrenfest dynamics with TDDFT

Recently, we developed an *ab initio* direct Ehrenfest dynamics scheme using a three time step integrator. The three different time steps are implemented with nuclear velocity Verlet,[14] a nuclear position coupled midpoint Fock integrator and a time-dependent Hartree-Fock with a modified midpoint and unitary transformation (MMUT) algorithm. All energies, gradients, and properties are generated directly as needed, or "on the fly." In the current work, we extend the implementation of the three time step integrator into a Kohn-Sham framework.

The TDDFT equation in matrix formulation is

$$i\frac{\partial \mathbf{P}}{\partial t} = \mathbf{KP} - \mathbf{PK}, \tag{1}$$

where $\mathbf{P}$ and $\mathbf{K}$ are the density and Kohn-Sham matrices, respectively, in an orthonormalized basis. Because the Kohn-Sham matrix is a function of instantaneous nuclear position and electron density, integration of Eq. (1) can often be split into propagations of slow nuclear and fast electronic motions, with time steps of Δt_N and Δt_e, respectively. Such a double split operator scheme can lead to significant integration errors if the time step is too large.[13] Our three time step

[a)]Author to whom correspondence should be addressed. Electronic mail: li@chem.washington.edu

integration technique introduces an intermediate propagator that assumes steady nuclear motion (constant acceleration) during Δt_{Ne}, and accordingly updates the nuclear positions in the integrals for the electronic density. We present here a brief summary of the methodology; for detailed machinery and in-depth discussion about the algorithm, we refer readers to Ref. 3.

The electronic degrees of freedom are propagated with the MMUT method.[15] The unitary transformation matrix is a time-evolution operator constructed from the eigenvectors $\mathbf{C}(t_k)$ and eigenvalues $\boldsymbol{\varepsilon}(t_k)$ of the Kohn-Sham matrix,

$$\mathbf{C}^{\dagger}(t_k)\cdot\mathbf{K}(t_k)\cdot\mathbf{C}(t_k)=\boldsymbol{\varepsilon}(t_k), \tag{2}$$

$$\begin{aligned}\mathbf{U}(t_k)&=\exp[i\cdot 2\Delta t_e\cdot\mathbf{K}(t_k)]\\&=\mathbf{C}(t_k)\cdot\exp[i\cdot 2\Delta t_e\cdot\boldsymbol{\varepsilon}(t_k)]\cdot\mathbf{C}^{\dagger}(t_k),\end{aligned} \tag{3}$$

where Δt_e is the time step for the MMUT integrator. The density matrix is then propagated from time t_{k-1} to t_{k+1} with a fixed nuclear position,

$$\mathbf{P}(t_{k+1})=\mathbf{U}(t_k)\cdot\mathbf{P}(t_{k-1})\cdot\mathbf{U}^{\dagger}(t_k). \tag{4}$$

By computing the Kohn-Sham matrix at the midpoint of the step, the MMUT method accounts for linear changes in the density matrix during the time step. This linearization will only be accurate for small time steps Δt_e, in which the density does not change much.

Because the electronic wave function changes much faster than the nuclear motion, the nuclear position coupled midpoint Kohn-Sham propagator updates integrals required in the Kohn-Sham matrix with the second kind of time step Δt_{Ne}, which encompasses m Δt_e iterations. The integrals are recomputed at the midpoint of every Δt_{Ne} time step, $t'+\Delta t_{Ne}/2$, and are used in the Kohn-Sham matrix $\mathbf{K}$ for the m MMUT steps between t' and $t'+\Delta t_{Ne}$,

$$\mathbf{K}(t)=\mathbf{h}\left[x\left(t'+\frac{\Delta t_{Ne}}{2}\right)\right]+\mathbf{G}_{xe}\left[x\left(t'+\frac{\Delta t_{Ne}}{2}\right),\mathbf{P}(t)\right], \tag{5}$$

where $\mathbf{h}$ and $\mathbf{G}_{xe}$ are one and two electron matrices, respectively. The nuclear position is updated for n Δt_{Ne} time steps before the gradient is recalculated, which occurs in the third time step $\Delta t_N=n\Delta t_{Ne}$. Velocity Verlet is used to propagate the nuclear coordinates,

$$p(t_{k+1/2})=p(t_k)-\tfrac{1}{2}g(t_k)\Delta t_N, \tag{6}$$

$$x(t_{k+1})=x(t_k)+\frac{p(t_{k+1/2})}{M}\Delta t_N, \tag{7}$$

$$p(t_{k+1})=p(t_{k+1/2})-\tfrac{1}{2}g(t_{k+1})\Delta t_N, \tag{8}$$

where p is the momenta and g is the energy gradient. The quantum mechanical gradient for noncommuting Kohn-Sham and density matrices, $[\mathbf{K},\mathbf{P}]\neq 0$, is generally different from Born-Oppenheimer dynamics.

B. Adaptive step size control

The use of a constant time step is not always computationally efficient. When the nonadiabaticity of the system is small (when electronic energy levels are spaced far apart), a large time step does not introduce significant integration errors. However, small time steps are necessary in regions of high nonadiabaticity. In order to reduce the overall computational cost, we introduce a simple technique to dynamically control the integration step size.

Instead of monitoring the rate of the potential change, we use the growth of energy conservation error as a direct measurement of integration quality. In our earlier paper,[13] we showed that the three time step propagator eliminates time-dependent Hartree-Fock integration errors if a large number of midpoint Fock steps is used. Here we instead focus on controlling the growth of the energy conservation error arising from the velocity Verlet step. The growth of energy conservation error at time t_k is defined as

$$\Delta E(t_k)=E(t_k)-E(t_{k-1}), \tag{9}$$

where E is the total energy of the system. The velocity Verlet method for classical dynamics has been shown to have a third order local truncation error and exhibits a second order growth of global errors,[16] i.e.,

$$\Delta E(t_k)\sim\Delta t^2, \tag{10}$$

where Δt is the velocity Verlet time step (Δt_N in the section above). Therefore, the rate of the local error growth should be first order with respect to Δt,

$$\Delta\dot{E}(t_k)=a\Delta t, \tag{11}$$

where the prefactor a depends on the rate of local potential surface change. A straightforward approach uses the local gradient to approximate the prefactor,

$$\Delta\dot{E}(t_k)\sim\dot{x}\Delta t\approx\Delta x. \tag{12}$$

Equation (12) is the working function in our adaptive step size control. Once the growth of error $\Delta E(t_k)$ is determined, the error at time t_{k+1} can be estimated,

$$\Delta E(t_{k+1}^{*})=\frac{\Delta E(t_k)}{\Delta\bar{x}(t_{k+1}^{*})}\Delta\bar{x}(t_k), \tag{13}$$

where $\Delta\bar{x}=\sqrt{\Sigma_{i=1}^{N}\Delta x_i^2}/N$ is the root-mean-square of changes of coordinates. This simple algorithm allows one to scale the time step [Eq. (12)] so that the upcoming error increase is within a preset bound.

In the current implementation, the upper and lower bounds for error growth are set to 10^{-6} and 10^{-7} a.u. of energy change per time step. If the energy change is outside of these bounds, we set Δt_N to be 0.005 and 0.25 fs as the lower and upper time step limits, respectively, to enhance the integration stability. The numbers of midpoint Kohn-Sham and MMUT-TDDFT steps are kept constant.

III. RESULTS AND DISCUSSION

The TDDFT Ehrenfest dynamics described above is implemented within the development version of the GAUSSIAN series of programs.[17] We apply the method to collisions of oxygen atoms and ions with graphite surfaces. This is a system of active experimental inquiry, and it serves as a challenging test of the method. Hydrogen terminated graph-

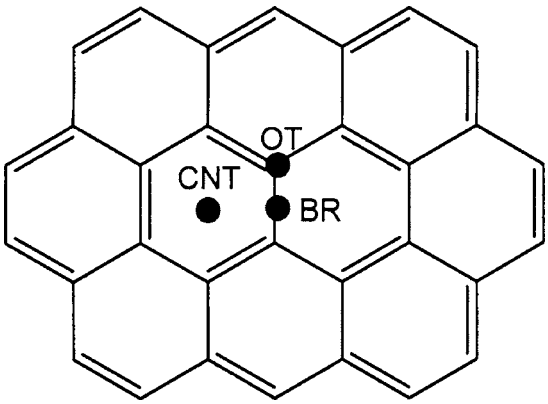

FIG. 1. Graphite cluster and three collision sites: on-top (OT), bridge (BR), and center (CNT).

ite clusters are used in the current study. The cluster, with corresponding collision sites, is shown in Fig. 1. Only the top (graphene) layer is included in the evolution of the electronic state. A second graphite layer is modeled with static charges. The geometry of the cluster is idealized to that of graphite with fixed 120° angles, 1.414 Å C–C bonds,[18] 1.07 Å C–H bonds, and a 3.255 Å interlayer distance between the cluster and the point charges. The Perdew, Burke, and Ernzerhof exchange and correlation functional density functional[16] is used in all calculations with valence electrons modeled with the STO-3G basis for perimeter carbons and hydrogen terminals, and the 6-31G basis for the atoms in the center of the cluster near the collision site. To decrease computing time and improve the electronic potential of the cluster surface, all core electrons are replaced with a modified Stuttgart MWB effective core potential.[19] The pseudopotential is scaled by 1.05 to improve the electronic properties of the graphite cluster by reproducing the experimental work function of graphite of 4.6 eV.[20] Point charges are included as a second layer obtained according to the CHELPG scheme[21] from calculations of a two layer cluster with a 6-31G basis. The HOMO-LUMO gap of resulting graphite cluster is 1.95 eV. The 6-31G basis with an unscaled Stuttgart MWB effective core potential is used for the colliding oxygen atoms. Relevant ionization potentials and electron affinities are in Table I.

We simulate collisions at three different positions: on top, bridge, and center graphite cluster sites (Fig. 1). During the simulation, the reference plane of the graphite cluster is kept steady by freezing the perimeter atoms and hydrogen terminals. Atoms involved in the collision site are allowed to propagate on the mean potential, allowing couplings between

TABLE I. Calculated ionization potentials and electron affinities for the various charge states of the graphite cluster and atomic oxygen.

Charge (spin)	State ΔE (eV)	Charge (spin)	State ΔE (eV)
Graphite (S)	0	Oxygen (T)	0
Graphite^{+} (D)	4.59	Oxygen^{+} (Q)	14.15
Graphite^{2+} (S)	13.10	Oxygen^{2+} (T)	50.06
Graphite^{-} (D)	0.87	Oxygen^{-} (D)	−0.92
Graphite^{2-} (S)	5.70	Oxygen^{2-} (S)	6.47

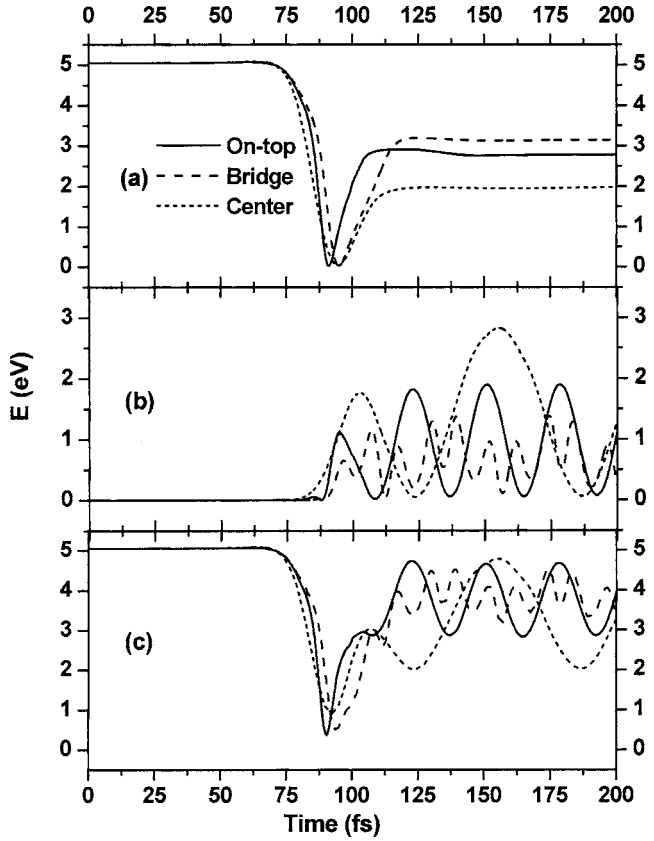

FIG. 2. Kinetic energies of (a) O(^3P), (b) the graphite cluster, and (c) the entire system.

electronic degrees of freedom and local nuclear vibrations within the TDDFT Ehrenfest dynamics framework. In the current study, only collisions normal to the graphite plane are considered. The dynamics are initiated with the oxygen atom with 5 eV of collision energy 8 Å away from the cluster, modeling the relative impact velocity of atomic oxygen with an orbiting spacecraft.[22,23] With the dynamic step size control velocity Verlet time step method introduced above, the average velocity Verlet time step is 0.045 fs. Within this time step, 5 steps of midpoint Kohn-Sham and 50 steps of MMUT-TDDFT are used. The total energy for all dynamics studies is conserved to within 0.01 kcal/mol.

Unlike O^{+}(^4S), where the electron distribution in the p shell is spherically symmetric, O(^3P) and O^{-}(^2P) p orbital occupancies are directionally dependent with respect to the graphite plane. Such orientational effects were studied with a smaller graphite cluster. We compared O(^3P) and O^{-}(^2P) dynamics for occupied and unoccupied p orbitals initially along the velocity direction (normal to the graphite plane) at the on-top site. The p-orbital occupancies of both O(^3P) and O^{-}(^2P) dynamically reorient at long range, leading to no significant differences in the energy or charge transfer during the collision process. Because of the single determinant representation of the wave function within the Ehrenfest dynamics, results are averaged over the p-orbital spatial orientations.

A. Collisions of O(^3P)

Figure 2 shows the time evolution of the kinetic energies

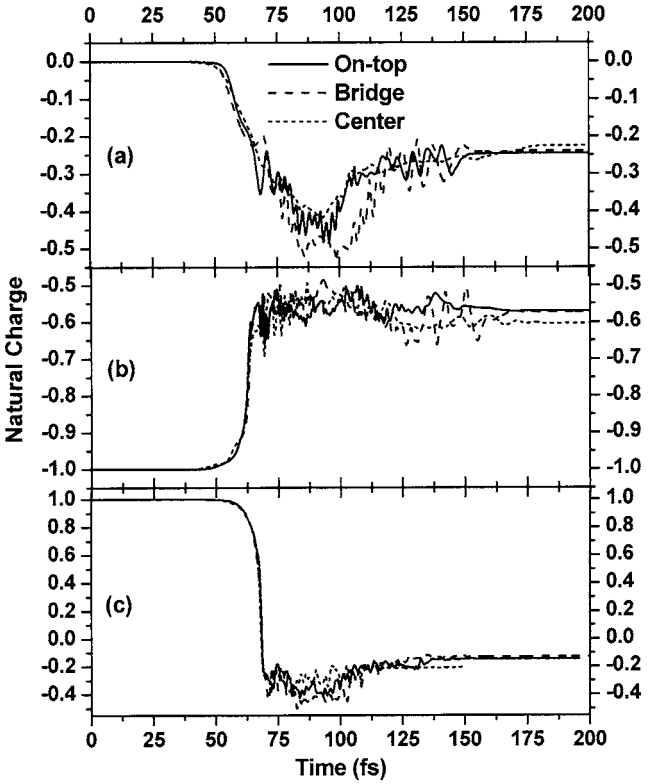

FIG. 3. Natural bond orbital charges on atomic oxygen for (a) $O(^3P)$, (b) $O^-(^2P)$, and (c) $O^+(^4S)$ during the course of the collision with the graphite cluster.

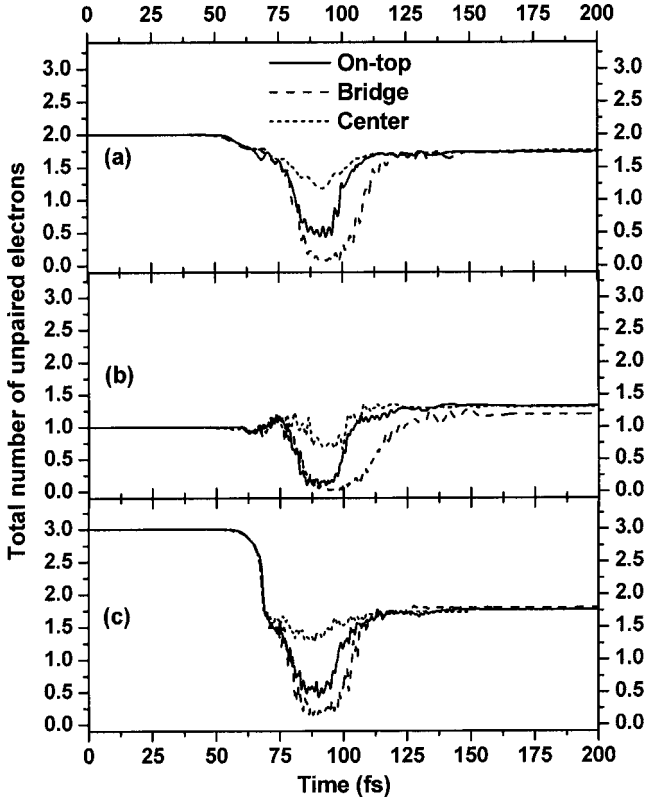

FIG. 4. Number of unpaired electrons on atomic oxygen for (a) $O(^3P)$, (b) $O^-(^2P)$, and (c) $O^+(^4S)$ during the course of the collision with the graphite cluster.

of neutral atomic oxygen (a), the graphite cluster (b), and the whole system (c). The dynamic behavior at the three collision sites is similar. At long range, the ground state simply corresponds to two neutral species, resulting in a steady kinetic energy and charge distribution from 0–50 fs or 8–3 Å apart. The oxygen velocity then decreases until it collides with the cluster at 1.2 Å, after which the oxygen atom bounces back with a final kinetic energy substantially less than the original value of 5 eV. The graphite cluster gains a total of 1.8 eV of energy from the collision with atomic oxygen at the bridge site, and 2.2 and 3.0 eV for those at on-top and center sites, respectively. The oscillations of the graphite kinetic energy [Fig. 2(b)] show that most of the gained energy is transferred into vibrations of the cluster, which are predominantly along the collision direction (z), rather than along carbon-carbon bonds (in the xy plane). The energy transferred into vibration is estimated to be 1.9 eV for on-top, 1.4 eV for bridge, and 2.8 eV for center site collisions. The graphite cluster of the center site gains the most energy, and has the largest kinetic energy oscillation amplitude. Because this collision site has six carbon atoms to share the impact of the collision along z (the on-top site has one, the bridge site has two), the frequency of the center oscillation is the lowest among the three sites.

As the oxygen gets closer to the graphite cluster, the character of the ground state of the system changes from O/graphite to the charged O^-/graphite$^+$, due to the strong Coulombic interaction which energetically favors charged species over neutral at close range. There are thus avoided crossings of these two states (estimated to occur at a distance between 3.5 and 4 Å based on the electron affinities and ionization potentials in Table I) and the O^{2-}/graphite^{2+} (estimated to cross between 3 and 2.5 Å) state. The charge oscillatory behavior [Fig. 3(a)] during the collision process indicates mixing of the various accessible electronic states as a result of electron-nuclear coupling in the form of nonadiabatic transitions.

The Coulombic attraction in the charge state is not strong enough to cause the 5 eV oxygen to permanently "stick" to the graphite surface. Instead, it bounces back to the noninteracting or weak interacting region ($>\sim 4$ Å), maintaining a partial charge of −0.25 from interaction with the graphite cluster. This superposition state at the asymptotic dissociation limit is not physically realistic. While the charge remaining on the oxygen when it is no longer interacting with the cluster is an artifact of the mean field Ehrenfest method that does not include decoherence of the superposition wave function, it nevertheless represents the overall average result of the nonadiabatic transition in the strong interaction region. If the system remained on a single adiabatic surface of varying charge character throughout the collision, the oxygen atom would have to return to the same final charge state when it bounced back from the cluster. Instead, the system propagates back on a mean field that includes some mixing of the charge separated state with the neutral state.

Figure 4 plots the number of unpaired electrons on atomic oxygen during the course of the collision with the graphite cluster. The neutral oxygen atom [Fig. 4(a)] starts

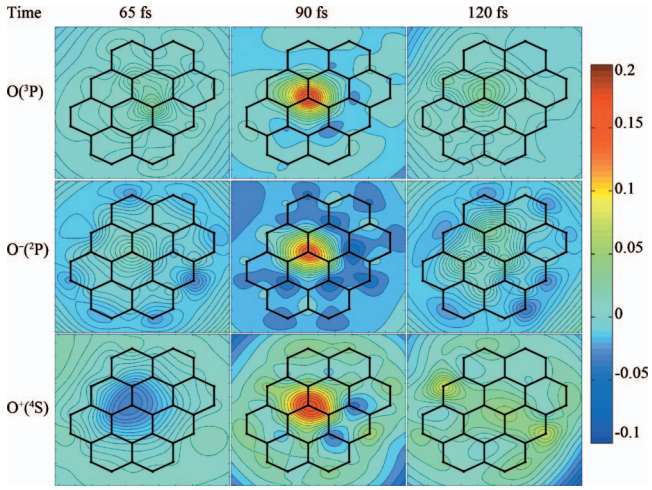

FIG. 5. (Color) Two-dimensional (2D) charge distributions of the graphite surface for collisions at the on-top site.

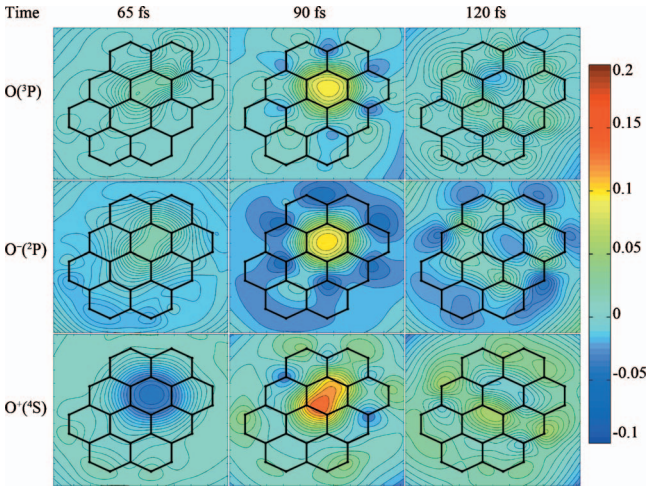

FIG. 7. (Color) 2D charge distributions of the graphite surface for collisions at the center site.

the dynamics in the $O(^3P)$ state. At the turning point, the oxygen atom shows significant singlet character at the on-top and bridge sites. The oxygen returns, however, to a predominantly triplet state after it bounces back from all collision sites. This return to the original spin state suggests that the graphite surface can retain the "memory" of the charge and spin states of collision atoms. This is certainly surprising because graphite is thought to behave like a metal which is generally assumed not to exhibit such memory. Contour plots of the charge distribution difference (compared to the $t=0$ fs charge distribution) provide more insights into electronic damage of the graphite cluster as a result of collision induced nonadiabatic charge transfer. Figures 5–7 plot charge distributions of the graphite cluster at three different critical times for collisions of the three oxygen species. Critical times are chosen as (1) 65 fs, when the oxygen starts entering the strong interaction region ($<\sim 3.0$ Å); (2) 90 fs, when the oxygen-graphite distance is the smallest (~ 1.2 Å); and (3) 120 fs, when oxygen has left the strong interaction region ($<\sim 2.9$ Å). Figures 5–7, top rows, show that the early charge transfer at 65 fs delocalizes the charge throughout the cluster, but the close interaction between the oxygen and the cluster at 90 fs (1.2 Å) is localized to the closest carbon atoms. The highly localized change in charge shows that the oxygen atom forms a seemingly covalent bond (π-lone pair interaction for the center collision case) with the local area of the surface, particularly at the bridge and on-top sites. Because the interaction is localized between the oxygen and participating carbons, the charge and spin states of the collision atom are retained. In contrast, if a metallic bond were formed between the colliding atom and a metal surface, charges are completely separated and can be dissipated into surface atoms and therefore the memory of the electronic state of the collision atom is expected to be lost. The graphite cluster thus behaves in a covalent fashion as the oxygen atom approaches the carbon surface, retaining the original electronic state of the oxygen during the local interaction.[24–26] We would thus expect and, indeed, find that oxygen atoms bouncing off the surface of a graphite cluster retain some memory of their original spin state.

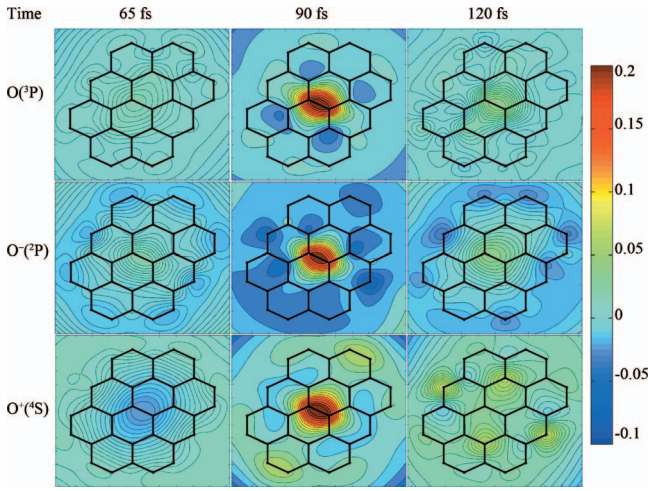

FIG. 6. (Color) 2D charge distributions of the graphite surface for collisions at the bridge site.

B. Collisions of $O^-(^2P)$

Because of the long range Coulombic repulsion between the negative charge on $O^-(^2P)$ and electron clouds of the graphite cluster, the kinetic energy of the oxygen atom begins to decrease much earlier in the dynamics than for $O(^3P)$. Other than this initial difference, the kinetic energy evolutions of $O^-(^2P)$ [Fig. 8(a)] and graphite [Fig. 8(b)] are very similar to those for the $O(^3P)$ atom case. The $O^-(^2P)$ bounces back with a loss of kinetic energy of ~ 2.0 eV, resulting in vibrations in the graphite surface. Collision at the center site once again transfers the most kinetic energy from the oxygen atom. The O/graphite$^-$ and the O^-/graphite potential energy surfaces are very close in energy at all distances. Electron-nuclear coupling leads to mixing between states, and as a result, the oxygen shows a loss of total electron density of about $0.4e$, as indicated in Fig. 3(b). As with the neutral collision, the anion interacts very locally with the graphite surface. Even though both the oxygen and the surface carry a negative charge, the interaction between the oxygen and the carbons of the collision is localized to make the

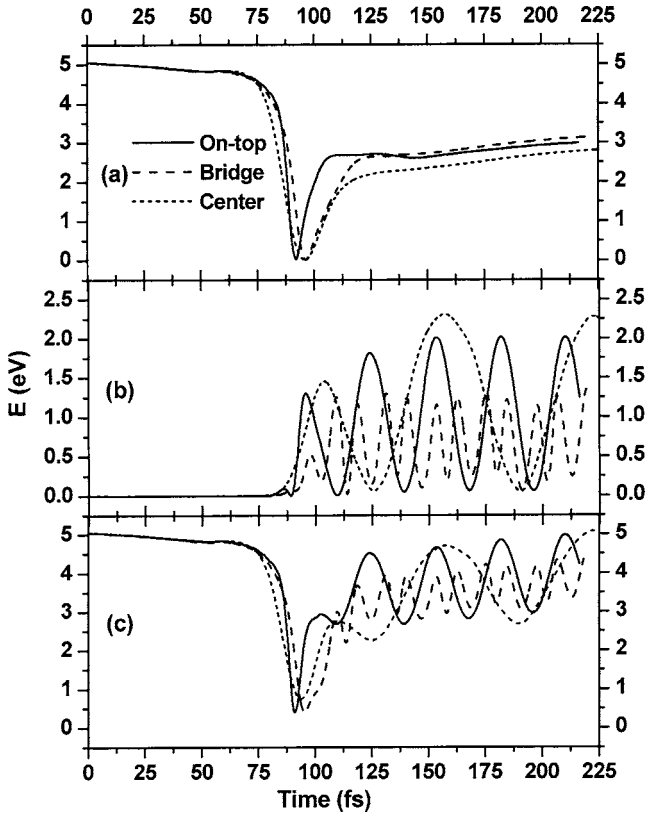

FIG. 8. Kinetic energies of (a) $O^-(^2P)$, (b) the graphite cluster, and (c) the entire system.

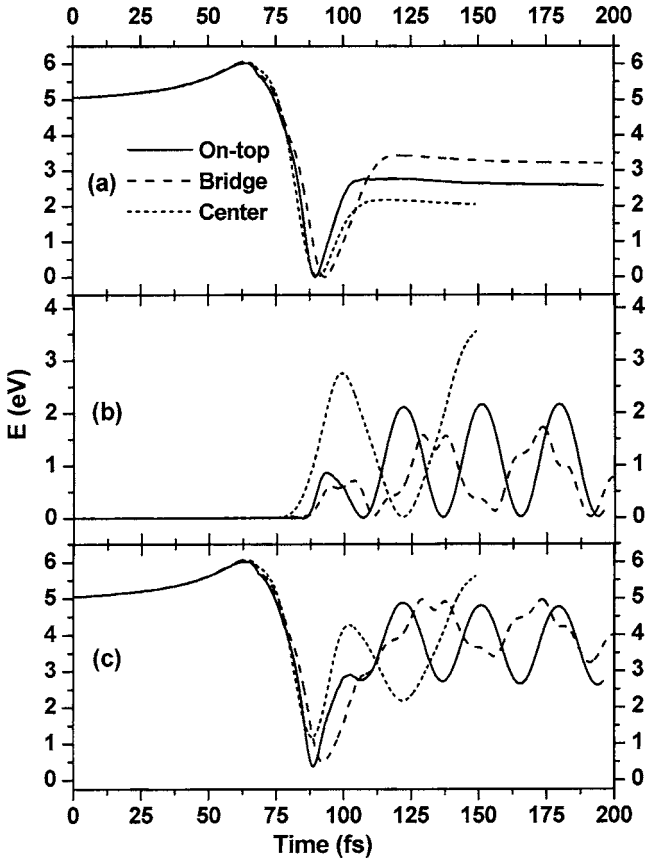

FIG. 9. Kinetic energies of (a) $O^+(^4S)$, (b) the graphite cluster, and (c) the entire system.

closest carbon atoms positively charged (Figs. 5–7, middle rows). Because of this local covalent interaction, the anion largely preserves its original doublet spin state after its singlet interaction (on-top and bridge sites) with the carbons [Fig. 4(b)].

C. Collisions of $O^+(^4S)$

In contrast to the $O(^3P)$ and $O^-(^2P)$ cases, the interaction of $O^+(^4S)$ with the electron clouds on the graphite surface is attractive, resulting in a long range attractive potential and an initial increase in kinetic energy [Fig. 9(a)]. The collision leads to a loss of oxygen kinetic energy of 1.8–3.0 eV, similar to the two cases discussed above. As before, the collision at the center site transfers more energy (~3.5 eV) to the surface than the other collision sites (1.8–2.2 eV). The charge transfer is rather significant compared to the $O(^3P)$ and $O^-(^2P)$ cases. The O^+/graphite state is much higher in energy than the O/graphite$^+$ and O^-/graphite^{2+} states because the electron affinities of O^+ and O are much higher than those of graphite$^+$ and graphite^{2+}, respectively. Coupling with these lower lying graphite ion states leads to the large degree of electron transfer ($1.2e$) from the graphite surface to the oxygen [Fig. 3(c)]. Because the coupling occurs with states that are lower in energy than the original charge state, the dynamics continue to propagate on a mean potential that is lower in energy than the original potential, leading to the corresponding release of extra potential energy into the kinetic energy of oxygen and vibrational energy of graphite cluster. The kinetic energy gain as a result of electronic relaxation to lower energy states is rather significant. The total kinetic energy of the cation system reaches 5.8 eV after the collision at the center site. Because of the change in the number of electrons, the cation cannot retain its original spin state [Fig. 4(c)]. So, unlike for the neutral and anionic states, the $O^+(^4S)$ in the center site collision undergoes a large change in its original spin state. Like the other oxygen species, $O^+(^4S)$ does not interact as a singlet at the center site as it does at the other two sites.

IV. CONCLUSIONS

In this paper, we introduce a new development of TDDFT Ehrenfest dynamics using a three time step propagator. This new methodology is able to describe electronically nonadiabatic processes and is efficient enough to be applied to dynamics simulations of atoms with surfaces. The method is applied to simulating collisions between atomic oxygen [$O(^3P)$, $O^-(^2P)$, and $O^+(^4S)$] and a graphite cluster for studies of the mechanisms of coupling between nuclear motion and electronic degrees of freedom, as in the erosion of surface materials of orbiting spacecraft by collision with atomic oxygen. Collisions at three different sites of the graphite cluster are modeled.

Although collision induced bond dissociation is not observed at the 5 eV collision energy modeled in this idealized graphite surface, our dynamical studies indicate that the local surface of the graphite cluster is vibrationally and electronically altered. In particular, we give the first report of incom-

plete loss of memory of the initial electronic state of the incident atom. The lasting change in charge on the atomic oxygen shows that, as a result of nuclear motion, the system has accessed lower energy electronic states with differing charge character. Among the three oxygen species studied, the oxygen cation introduces the most electronic damage to collision with the graphite surface. Qin *et al.* have studied bombardment of both decanethiolate and perfluorodecanethiolate self-assembled monolayers with atomic oxygen cations.[27] At the 5 eV incident O^+ energy comparable to our dynamics runs, the most common ionic products show the charge transfer from O^+ to the monolayer, agreeing with our observation of the charge inversion of O^+.

We give the first report of incomplete loss of memory of the initial electronic state of the incident atom. Strong local electronic damage was observed to be quickly distributed over several adjacent cells. The quick neutralization is indicative of a conducting surface. The graphite cluster, however, has a band gap of 1.95 eV, which shows that our model is by no means metallic. The nature of the interaction becomes covalent when the oxygen closely approaches the carbons of the surface. Unlike the initial rapid charge transfer, the electrons involved in this covalent contact are never significantly dissipated into the surface. As a result, the charge and electronic state of the colliding atom are partially retained.

ACKNOWLEDGMENTS

Support from the University of Washington Royalty Research Fund, AFOSR MURI (Grant No. F49620-01-1-0335), and NSF (Grant Nos. CHE-0314208 and CHE-0342956) is gratefully acknowledged.

[1] K. Bolton, W. L. Hase, and G. H. Peslherbe, in *Modern Methods for Multidimensional Dynamics Computation in Chemistry*, edited by D. L. Thompson (World Scientific, Singapore, 1998).
[2] R. Car and M. Parrinello, Phys. Rev. Lett. **55**, 2471 (1985).
[3] M. Tuckerman, B. J. Berne, and G. J. Martyna, J. Chem. Phys. **97**, 1990 (1992).
[4] E. Deumens, A. Diz, R. Longo, and Y. Ohrn, Rev. Mod. Phys. **66**, 917 (1994).
[5] M. C. Payne, M. P. Teter, D. C. Allan, T. A. Arias, and J. D. Joannopoulos, Rev. Mod. Phys. **64**, 1045 (1992).
[6] D. K. Remler and P. A. Madden, Mol. Phys. **70**, 921 (1990).
[7] D. Marx and J. Hutter, in *Modern Methods and Algorithms of Quantum Chemistry*, edited by J. Grotendorst (John vonNeumann Institute for Computing, Julich, 2000), Vol. 1, p. 301.
[8] H. B. Schlegel, J. M. Millam, S. S. Iyengar, G. A. Voth, A. D. Daniels, G. E. Scuseria, and M. J. Frisch, J. Chem. Phys. **114**, 9758 (2001).
[9] J. M. Millam, V. Bakken, W. Chen, W. L. Hase, and H. B. Schlegel, J. Chem. Phys. **111**, 3800 (1999).
[10] B. Corrigall, B. Kuppers, and R. Wallace, Phys. Rev. A **4**, 977 (1971).
[11] D. A. Micha, J. Phys. Chem. A **103**, 7562 (1999).
[12] D. A. Micha and K. Runge, Phys. Rev. A **50**, 322 (1994).
[13] X. Li, J. C. tully, H. B. Schlegel, and M. J. Frisch, J. Chem. Phys. **123**, 084106 (2005).
[14] L. Verlet, Phys. Rev. **159**, 98 (1967).
[15] X. Li, S. M. Smith, A. N. Markevitch, D. A. Romanov, R. J. Levis, and H. B. Schlegel, Phys. Chem. Chem. Phys. **7**, 233 (2005).
[16] J. P. Perdew, K. Burke, and Y. Wang, Phys. Rev. B **54**, 16533 (1996).
[17] M. J. Frisch, G. W. Trucks, H. B. Schlegel *et al.*, GAUSSIAN, Development Version, Gaussian, Inc., Wallingford, CT, 2004.
[18] S. J. Clark, J. Crain, and G. J. Ackland, Phys. Rev. B **55**, 14059 (1997).
[19] M. Dolg, U. Wedig, H. Stoll, and H. Preuss, J. Chem. Phys. **86**, 866 (1987).
[20] A. R. Ubbelohde and P. L. Walker, *Graphite and its Crystal Compounds* (Oxford University Press, London, 1960).
[21] C. M. Breneman and K. B. Wiberg, J. Comput. Chem. **11**, 361 (1990).
[22] J. D. Guthrie, C. Cerbus, E. S. Berman, and L. Rea, Advanced Materials and Processes Technology Information Analysis Center (AMPPTIAC) Quarterly **8**, 25.
[23] B. A. Banks, K. K. d. Groh, E. Baney-Barton, E. Edward, and A. Sechkar, SAE Tech. Pap. Ser. **1**, 2695. (1999).
[24] D. C. Jacobs, J. Phys.: Condens. Matter **7**, 1023 (1995).
[25] D. C. Jacobs, Annu. Rev. Phys. Chem. **53**, 379 (2002).
[26] J. C. Tully, Annu. Rev. Phys. Chem. **51**, 153 (2000).
[27] X. Qin, T. Tzvetkov, and D. C. Jacobs, J. Phys. Chem. A **110**, 1408 (2006).